Gate-controlled electron *g* factor in an InAs-inserted-channel $In_{0.53}Ga_{0.47}As/In_{0.52}Al_{0.48}As$ heterostructure

Junsaku Nitta,[a] Yiping Lin, and Tatsushi Akazaki
NTT Basic Research Laboratories, NTT Corporation, CREST, Japan Science and Technology Agency (JST), 3-1 Wakamiya, Morinosato, Atsugi-shi, Kanagawa 243-0198, Japan

Takaaki Koga
NTT Basic Research Laboratories, NTT Corporation, PRESTO, Japan Science and Technology Agency (JST), 3-1 Wakamiya, Morinosato, Atsugi-shi, Kanagawa 243-0198, Japan

(Received 2 June 2003; accepted 8 October 2003)

The electron *g* factor in an InAs-inserted-channel $In_{0.53}Ga_{0.47}As/In_{0.52}Al_{0.48}As$ heterostructure is studied by measuring the angle dependence of magnetotransport properties. The gate voltage dependence of the *g* factor is obtained from the coincidence method. The *g*-factor values are surprisingly smaller than the *g*-factor value of bulk InAs, and close to the bare *g*-factor value of $In_{0.53}Ga_{0.47}As$. A large change in the *g* factor is observed by applying the gate voltage. The gate voltage dependence is not simply explained by the energy dependence of the *g* factor. © *2003 American Institute of Physics.* [DOI: 10.1063/1.1631082]

The electron *g* factor is of fundamental importance for the electronic band structure in semiconductors as well as for spin-related devices. Recently, much attention was focused on the *g*-factor engineering for processing of quantum information based on the electron spin degree of freedom.[1] The gate controlled *g* factor has been demonstrated in GaAs/AlGaAs systems by time-resolved Kerr rotation measurements[2] and by the electron spin resonance,[3] since a carrier wave-function penetrates into the barrier material with a different *g* factor from that of the quantum well resulting in a different contribution to the *g* factor.

The coincidence method,[4] where the tilt angle dependence of Shubnikov–de Haas (SdH) oscillations is measured, has often been used to deduce the *g* factor in two-dimensional electron gas (2DEG), e.g., in an InAs–AlSb quantum well,[5] an InAs–GaSb superlattice,[6] an InAs–GaSb quantum well,[7] and an InGaAs/InAlAs quantum well.[8] An InAs-inserted-channel $In_{0.53}Ga_{0.47}As/In_{0.52}Al_{0.48}As$ heterostructure is an interesting system from the view point of *g*-factor engineering. The smaller band offset at the interface between InAs and $In_{0.53}Ga_{0.47}As$ than in usual $In_{0.53}Ga_{0.47}As/In_{0.52}Al_{0.48}As$ or $In_{0.53}Ga_{0.47}As/InP$ heterostructures makes the wave-function penetration easier. Furthermore, the InAs channel is not lattice matched to the $In_{0.53}Ga_{0.47}As$. The band structure in semiconductors is influenced by strain effects due to the lattice mismatch, but it is not well understood how the *g* factor is affected by the strain. In this letter, we study the gate voltage dependence of *g*-factor values of this InAs-inserted-channel $In_{0.53}Ga_{0.47}As/In_{0.52}Al_{0.48}As$ heterostructure. The *g*-factor values are obtained from the coincidence method under the condition where the exchange enhancement of the *g* factor is negligible. A large modulation of the *g* factor is observed by applying the gate voltage.

The sample is an inverted-doped InAs step quantum well with 25-nm-$In_{0.52}Al_{0.48}As$ cap layer. The step quantum well is composed of 13.5-nm-$In_{0.53}Ga_{0.47}As$, an inserted 4-nm-InAs channel, and a 2.5-nm-$In_{0.53}Ga_{0.47}As$ layer. Underneath the quantum well is a 20-nm-spacer layer of $In_{0.52}Al_{0.48}As$ on top of 7-nm-thick Si-doped-$In_{0.52}Al_{0.48}As$ layer. The doping density of 7-nm-thick $In_{0.52}Al_{0.48}As$ carrier supplying layer is 4×10^{18} cm^{-3}. The sample was grown by molecular beam epitaxy after $In_{0.52}Al_{0.48}As$ buffer layer growth on Fe-doped semi-insulating (100) InP. All $In_{0.53}Ga_{0.47}As$ and $In_{0.52}Al_{0.48}As$ layers are lattice matched to InP, while the 4-nm-InAs-inserted layer is not matched and strained. It has been reported that the mobility is highest when the thickness of InAs is 4 nm and starts to decrease above the thickness of 5 nm InAs since the thickness of 4 nm InAs is less than the critical thickness.[9] Shown in Fig. 1(a) is the potential profile and squared wavefunction obtained by a self-consistent Poisson–Schrödinger calculation.

A 20×80 μm^2 Hall bar sample was made by the typical photolithography technique. The gate electrode was deposited on top of the 100-nm-thick Al_2O_3 insulating layer that covers the entire area of the Hall bar. All transport measurements were performed in a ^{3}He cryostat equipped with a 9 T superconducting magnet, where the magnetic field was applied at a tilt angle from perpendicular to the heterointerface.

Figure 1(b) shows a gray-scale plot of $R_{xx}(B,V_g)$ data presenting a Landau fan diagram, where the magnetic field B is applied perpendicular to the 2DEG plane. In this figure, ν is the filling factor and is determined by comparing with Hall resistance $R_{xy}(V_g)$. The carrier concentration N_s and the electron mobility μ were changed from 8.3×10^{11} cm^{-2} and 66 000 cm^2/Vs at $V_g=-5$ V to 1.9×10^{12} cm^{-2} and 119 000 cm^2/Vs at $V_g=5$ V. The effective mass was $m^*=0.041m_0$ at $V_g=-3$ V and $m^*=0.044m_0$ at $V_g=3$ V as determined from the temperature dependence of the SdH-oscillation amplitude. Here, m_0 is the free-electron mass. The experimentally obtained m^* values are consistent with the previous study.[10] From these analyses, the Fermi energy E_F was esti-

[a]Electronic mail: nitta@will.brl.ntt.co.jp

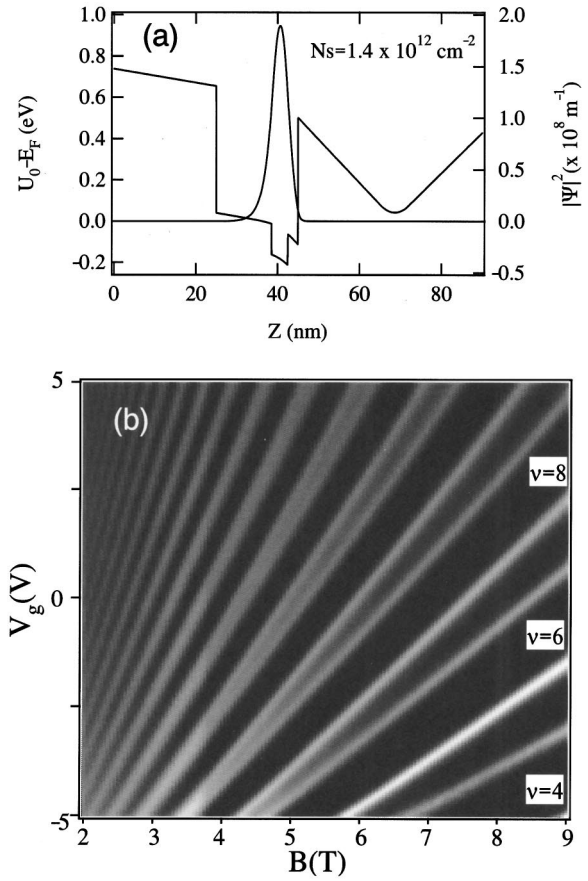

FIG. 1. (a) Calculated potential profile and squared wavefunction of the InAs-inserted-channel InGaAs heterostructure at $N_s=1.4\times10^{12}$ cm^{-2}. U_0 is a potential energy. (b) Gray-scale plot of $R_{xx}(B,V_g)$ data. Black (white) areas indicate small (large) values of the resistance R_{xx}. ν is the filling factor. A clear spin splitting develops above 5 T.

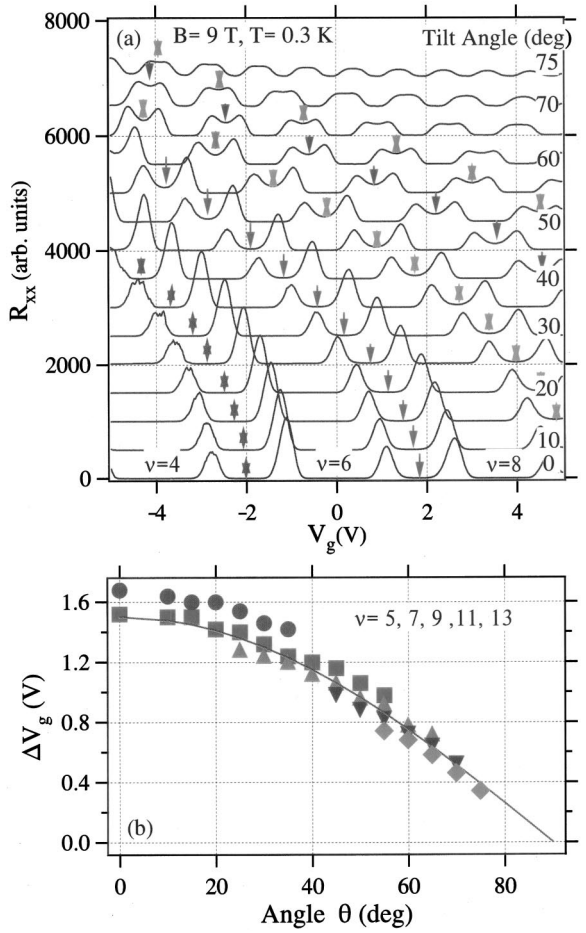

FIG. 2. (a) R_{xx}-V_g data for various tilt angles θ from 0° to 75° in 5° steps. Data are shifted for clarity. Arrows show the odd filling factor positions. (b) Gate voltage spacing ΔV_g as a function of tilt angle. The gate voltage spacing ΔV_g around the odd filling factors is determined from the splitted peak positions in R_{xx}-V_g data. The solid line shows the cos θ dependence for comparison. The filled circles, squares, triangles, inverse triangles, and diamonds correspond to data obtained for $\nu=5$, 7, 9, 11, and 13, respectively.

mated to be 49 meV at $V_g=-5$ V and 101 meV at $V_g=5$ V.

The Landau level spectrum is given by

$$E_n=E_0+\hbar\omega_c\left(n+\frac{1}{2}\right)\pm\frac{1}{2}g\mu_B B, \tag{1}$$

where E_0 is the subband energy, $\hbar$ the Planck's constant, ω_c the cyclotron frequency, n the Landau index, and μ_B the Bohr magneton. The resistance peak (white curves) in the $R_{xx}(B,V_g)$ plot satisfies the relation $E_n=E_F$. The filling factor ν, where SdH oscillations show spin splitting, is around 15.

For 2DEG in large perpendicular magnetic fields, when there are unequal populations of electrons with opposite spins, the electron–electron interaction can lead to a substantial enlargement of the spin splitting energy, which can be attributed to an enhancement of the effective g factor.[11] Figure 2(a) shows R_{xx}-V_g data for various tilt angles θ. Well-separated spin splitting was observed at $\theta=0°$, and may be due to the enhancement of the g factor. However, spin splitting became unclear at higher tilt angle θ. The tilt angle θ is defined with respect to the surface normal ($\theta=0$). In Fig. 2(b), gate voltage spacing ΔV_g values separated by the spin splitting are plotted as a function of tilt angle. Here, ΔV_g was determined from two peak positions of R_{xx} around the odd filling factors. The ΔV_g values show nearly cos θ dependence.

The electron g factor was determined from the coincidence method. The Zeeman splitting is proportional to the total magnetic field B_{total}, whereas the Landau splitting is proportional to the component of the field perpendicular to the 2DEG, $B_{\text{per}}=B_{\text{total}}\cos\theta$. The ratio between the Landau splitting and the Zeeman spin splitting is given by

$$r=\frac{g\mu_B B_{\text{total}}}{\hbar\omega_c}, \tag{2}$$

where $\omega_c=eB_{per}/m^*$. The first minima of the SdH oscillations appears at $r=1/2$ when the tilt angle θ_c satisfies the condition

$$\cos\theta_c=g\frac{m^*}{m_0}. \tag{3}$$

In the above coincident analysis, for simplicity, we neglect the zero field spin splitting due to the Rashba spin–orbit interaction since SdH oscillations do not show clear beating in a low magnetic field.

Shown in Fig. 3(a) are $R_{xx}(B_{per})$ traces for various tilt angles θ. The SdH-oscillation amplitude decreases with increasing tilt angle, and the minima appear around $\theta=80.6°$. Further increase of the tilt angle leads to the swap-

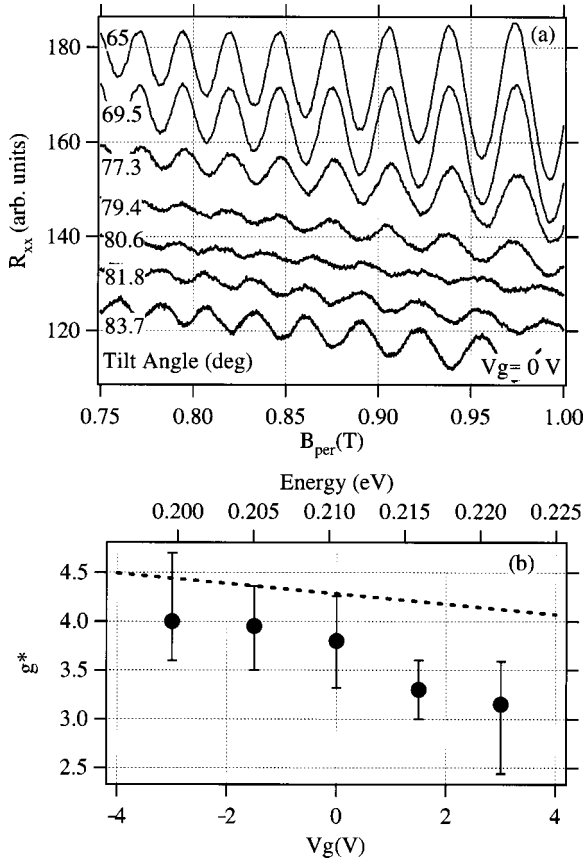

FIG. 3. (a) Magnetoresistance R_{xx} at $V_g=0$ V vs the perpendicular component of magnetic fields for various tilt angles. The tilt angle is increased from the top (65°) to the bottom (83.7°). Data are shifted for clarity. (b) Gate-voltage dependence of the g factor. The dotted line corresponds to calculated g-factor values. Top x axis indicates the energy from the conduction band edge of InAs. Note that the sign of the g factor cannot be determined from the coincidence method. The calculated g-factor values are negative, but their absolute values are plotted.

ping of the SdH oscillation phase and an increase of the amplitude. From the values of θ_c and m^*, $|g^*|=3.8$ is obtained according to Eq. (3). Figure 3(b) shows the gate voltage dependence of the g^* values. These g^* values are much smaller than the g factor of bulk InAs. In our case, the exchange enhancement may be negligible since we obtained the g factor at filling factors much larger than the critical filling factor ν_c, where the collapse of exchange enhancement occurs. When the energy separation of spin-up and -down levels is less than their disorder broadening, the exchange contribution will disappear and only the bare Zeeman splitting will remain.[12]

The energy dependence of the g factor[13] is given by

$$g(E)=g_0-\frac{4}{3}\frac{P_{cv}^2}{m_0}\frac{\Delta_{so}}{(E_g+E)(E_g+\Delta_{so}+E)}, \qquad (4)$$

where E is the energy from the conduction band edge, E_g the band gap, g_0 the free electron g factor, Δ_{so} the spin-orbit splitting of the valence band, and $2p_{cv}^2/m_0$ the interband matrix element of the momentum operator. The regime of the g factor described by Eq. (4) ranges from -14.8 for bulk InAs to 2.0023 for free electrons. The dotted line in Fig. 3(b) is a calculation of the g factor according to the equation:

$$g_{\text{total}}(E)=g_{\text{InAs}}(E)\langle\Phi_{\text{InAs}}\rangle+g_{\text{InGaAs}}(E)\langle\Phi_{\text{InGaAs}}\rangle, \qquad (5)$$

where $\langle\Phi\rangle$ is the probability of finding an electron either in InAs or $In_{0.53}Ga_{0.47}As$. The calculated g-factor values are negative, but their absolute values are plotted. These probabilities were calculated by solving the Poisson and Schrödinger equations self-consistently. The calculated probability $\langle\Phi_{\text{InAs}}\rangle$ changes from 68% at $V_g=-5$ V to 63% at $V_g=5$ V. In this calculation, we assume that the band offset at the interface between InAs and $In_{0.53}Ga_{0.47}As$ is 0.15 eV. In Fig. 3(b), the top x axis indicates the energy from the conduction band edge, considering the confinement energy in the InAs quantum well. Here, we use the values of the interband matrix element, the band gap, and the spin-orbit splitting of bulk $In_{0.53}Ga_{0.47}As$, which are $2p_{cv}^2/m_0=25.5$ eV, $E_g=0.813$ eV, and $\Delta_{so}=0.356$ eV, respectively.[14] The energy gap in the strained InAs is calculated to be $E_g=0.593$ eV based on a semi-empirical relation.[15] We assume $2p_{cv}^2/m_0=24$ eV and $\Delta_{so}=0.4$ eV for the strained InAs by interpolation between bulk InAs and $In_{0.53}Ga_{0.47}As$. The calculation qualitatively explains the gate voltage dependence of the g factor deduced from the coincidence method. However, two quantitative discrepancies are observed: the experimentally obtained g-factor values are smaller than the calculated values, and the change in the g factor by the gate is larger than in the above model calculation. More detailed information, such as band-structure properties and the band offset, about this strained InAs system is necessary in order to explain the experimental data.

In summary, the angle dependence of magnetotransport properties was investigated in an InAs-inserted-channel $In_{0.53}Ga_{0.47}As/In_{0.52}Al_{0.48}As$ heterostructure. The gate voltage dependence of the g factor was obtained from the coincidence method. The obtained g-factor values are surprisingly smaller than the value of the g factor of bulk InAs. The change of the g factor by the gate voltage in this system is much larger than in the GaAs/AlGaAs system.[3]

[1] H. Kosaka, A. A. Kiselev, F. A. Barton, K. W. Kim, and E. Yablonovitch, Electron. Lett. **37**, 464 (2001).
[2] G. Salis, Y. Kato, K. Ensslin, D. C. Driscoll, A. C. Gossard, and D. D. Awschalom, Nature (London) **414**, 619 (2001).
[3] H. W. Jiang and E. Yablonovitch, Phys. Rev. B **64**, R041307 (2001).
[4] F. F. Fang and P. J. Stiles, Phys. Rev. **174**, 823 (1968).
[5] S. Brosig, K. Ensslin, A. G. Jansen, C. Nguyen, B. Brar, M. Thomas, and H. Kroemer, Phys. Rev. B **61**, 13045 (2000).
[6] L. L. Chang, E. E. Mendez, N. J. Kawai, and L. Esaki, Surf. Sci. **113**, 306 (1982).
[7] T. P. Smith and F. F. Fang, Phys. Rev. B **35**, 7729 (1987).
[8] R. J. Nicholas, M. A. Brummell, J. C. Portal, K. Y. Cheng, A. Y. Cho, and T. P. Pearsall, Solid State Commun. **45**, 911 (1983).
[9] T. Akazaki, K. Arai, T. Enoki, and Y. Ishii, IEEE Electron Device Lett. **13**, 325 (1992).
[10] T. Akazaki, J. Nitta, H. Takayanagi, T. Enoki, and K. Arai, J. Electron. Mater. **25**, 745 (1996).
[11] R. J. Nicholas, R. J. Haug, K. von Klitzing, and G. Weimann, Phys. Rev. B **37**, 1294 (1988).
[12] D. R. Leadley, R. J. Nicholas, J. J. Harris, and C. T. Foxon, Phys. Rev. B **58**, 13036 (1998).
[13] A. A. Kiselev, E. L. Ivchenko, and U. Rössler, Phys. Rev. B **58**, 16353 (1998).
[14] E. L. Ivchenko, A. A. Kiselev, and M. Willander, Solid State Commun. **102**, 375 (1997).
[15] L. Hrivnák, Phys. Status Solidi A **123**, 133 (1999).